Received 15 July 2025, accepted 10 August 2025, date of publication 13 August 2025, date of current version 19 August 2025.

Digital Object Identifier 10.1109/ACCESS.2025.3598642

RESEARCH ARTICLE

Electromagnetic Characterization of Concrete by Jonscher Universal Dielectric Model: Numerical Validation of Different Nonlinear Optimization Algorithms

GIOVANNI ANGIULLI[1], (Senior Member, IEEE), AND MARIO VERSACI[2], (Senior Member, IEEE)

[1]Department of Information Engineering, Infrastructures and Sustainable Energy, Mediterranea University of Reggio Calabria, 89124 Reggio Calabria, Italy

[2]Department of Civil, Energetic, Environmental and Material Engineering, Mediterranea University of Reggio Calabria, 89124 Reggio Calabria, Italy

Corresponding author: Giovanni Angiulli (giovanni.angiulli@unirc.it)

This work was supported by Italian Ministry of University and Research under the Program Progetti di Rilevante Interesse Nazionale (PRIN) 2022: "Integration of Artificial Intelligence and Ultrasonic Techniques for Monitoring Control and Self-Repair of Civil Concrete Structures (CAIUS)."

ABSTRACT The dielectric permittivity model of concrete plays a key role in characterizing its interaction with electromagnetic (EM) waves but also in determining its mechanical properties. Among various EM models, the Jonscher universal dielectric response has been favored by scientists and practitioners in the field for the above purposes. Despite its widespread use, to the best of our knowledge, no study has focused its attention on the problem of choosing the most appropriate numerical method and the related starting point solution to solve the nonlinear least squares problem for fitting the Jonscher model to the experimental data. In this work, considering their broad adoption within software packages such as R, Python, or MATLAB, the performances of the Nelder-Mead, the Broyden-Fletcher-Goldfarb-Shanno, and the Levenberg-Marquardt nonlinear optimization algorithms have been compared among them to obtain practical guidance on which nonlinear optimization procedure to choose and how to generate a valid initial guess solution to achieve optimal fitting with the experimental data.

INDEX TERMS Concrete, complex dielectric permittivity, Jonscher model, optimization-based methods.

I. INTRODUCTION

As the most widely used building material, monitoring concrete properties is essential to assess its performance [1], prevent structural failures [2], ensure the durability of built structures, and optimize related maintenance efforts [3], [4], [5]. Among the various technologies designed to fulfill the aforementioned purposes, electromagnetic techniques offer the possibility of contactless and wireless real-time monitoring of building structures, as well as the ability to perform in-situ measurements [6], [7], [8], [9]. The orientation towards using the electromagnetic approach for monitoring concrete properties stems from the fact that, over the years, numerous studies have demonstrated the usefulness of electromagnetic-based approaches for its characterization [10], [11], [12], [13], and pointed out the existence of relationships between near-field microwave reflection analysis and concrete properties, such as water content [14], porosity [15], chloride presence [16], [17], and compressive strength, which is the most important parameter to describe its mechanical performance [18], [19], [20], for which machine learning based method have been also exploited [21], [22], [23]. Based on what has been discussed so far, it is clear that modeling the dielectric permittivity of concrete plays a pivotal role in characterizing the interaction of EM waves with this material as well as in determining its mechanical properties. Studies on the dielectric properties of concrete have received significant

The associate editor coordinating the review of this manuscript and approving it for publication was Li He.

attention in civil engineering [24], [25], [26]. Over the years, different permittivity models have been used in the literature to describe its dielectric response, such as Debye, complex refractive index method (CRIM), first-order exponential, and Cole-Cole model [10], [18], [24], [26]. Among others, the Jonscher universal dielectric response [27] introduced to model the permittivity of a wide variety of solid materials has also been exploited [28], [29], [30], [31], [32], [33]. The Jonscher model, being a more comprehensive permittivity model [34], [35], [36], [37], has met with favor among scholars and professionals in the field; it was employed to evaluate the concrete shielding effectiveness, obtaining better results compared with the Debye model ones [29], and to describe the dielectric permittivity of Chinese standard concrete [30], which is the most widely produced type of concrete in the world [38].

To determine the characteristic parameters of the Jonscher model, an appropriate nonlinear least-squares problem (NLSP) must be solved to fit the model to concrete permittivity-measured data [31], [39]. To this aim, a nonlinear optimization procedure must be employed to obtain the least-squares fit, and a starting solution (or initial guess) must be provided [40], [41]. It is well known that the choice of the initial guess solution for solving an NLSP must be based on all the information about the problem under consideration [40], [41]. The better the initial guess, the faster the convergence of the corresponding solution algorithm will be [41]. In addition to this aspect, it must be considered that a nonlinear least squares problem may have several local minima, where an inadequate initial value may lead to convergence to an undesired stationary point with physically impossible parameter values or to a solution that is not the absolute minimum for the problem at hand [41], [42]. Accordingly, choosing an initial guess solution is a predominant aspect of obtaining an accurate fitting model [42]. However, existing works on Jonscher parametrization have either applied numerical optimization without a systematic discussion of algorithm selection, initial guess sensitivity, or robustness to data noise (e.g., [31]) or adopted an analytical approach (e.g., [28]) exclusively suitable in case of the noiseless data.

Accordingly, based on the aforementioned considerations, the paper's aims are twofold:

i) comparing the numerical performance of the Nelder-Mead, Broyden-Fletcher-Goldfarb-Shanno (BFGS) quasi-Newton, and Levenberg-Marquardt nonlinear optimization algorithms applied to the determination of the best parameters for the Jonscher model;
ii) provides a rule for calculating the initial guess solution and evaluating its effectiveness as an input for these nonlinear optimization algorithms.

Several reasons guided our choice about the NLSP resolution methods considered in this study: first, these methods are widely recognized as standard references for nonlinear optimization [40], [41]. While newer nonlinear optimization algorithms are promising [43], [44], they often lack standardized implementations or require high computational resources that are not justified for small-sized problems, such as the one under consideration [41]. Second, these nonlinear procedures are integrated into widely used tools, such as MATLAB©, Python-SciPy, and R, as well as optimized libraries, which facilitates their adoption by researchers and practitioners in the field of electrical and civil engineering [45], [46].

The organization of this paper is as follows: Section II describes the theoretical framework of the Jonscher universal dielectric model. The problem formulation, the nonlinear optimization algorithms selected for the numerical resolution, and the rule to obtain an initial guess solution for the Nelder-Mead, BFGS, and Levenberg-Marquardt algorithms are described in Section III. In section IV, numerical simulation to evaluate the performance of the selected nonlinear optimization methods using synthetic and real concrete complex permittivity data are shown. Section IV presents some considerations based on the results of the conducted simulations.

II. THE JONSCHER UNIVERSAL DIELECTRIC MODEL

Accurately modeling dielectric permittivity in highly heterogeneous or complex materials such as concrete, rocks, soils, and polymers is a longstanding challenge in material science [42], [47]. It is worth noting that scattering mechanisms, both intrinsic and extrinsic, arising from microstructural heterogeneities can significantly affect the real and imaginary components of the electromagnetic response, particularly in heterogeneous materials [48]. Alternative models, such as the Lorentz oscillator and Wemple-DiDomenico dispersion relations, have been successfully employed for crystalline materials [49]. In contrast, the Jonscher universal model, considered here, is better suited for concrete, which can be considered a disordered heterogeneous system for which relaxation mechanisms are distributed and not associated with sharp resonances. The Jonscher universal dielectric model [27] provides a basis for describing with remarkable consistency the frequency-dependent behavior of the complex dielectric permittivity $\epsilon(\omega)$ in the matter, whose underlying logic, rooted in empirical observations across a wide variety of materials and frequency ranges, is based on the identified commonality in the frequency-dependent dielectric behavior of many disordered materials, regardless of their chemical composition or structural characteristics [27], [36]. More precisely, the Jonscher model explains the dielectric behavior of materials by modeling the relaxation processes occurring across different time scales through a power-law model, which is derived by replacing the concept of distribution of relaxation times used in the Debye or Cole-Cole models with the idea of the frequency-independent ratio of energy lost per cycle to energy stored [34], [35], [36]. The starting point for the formal introduction of the Jonscher model is the relation between the dielectric displacement vector D and the electric field $\mathbf{E}$ in an isotropic solid material, i.e., [27], [34]:

$$\mathbf{D} = \epsilon(\omega)\mathbf{E} = (\epsilon_0\chi(\omega) + \epsilon_\infty)\,\mathbf{E} \tag{1}$$

where ϵ_0 is the permittivity of the free space, ϵ_∞ is the $\epsilon(\omega)$ high-frequency limit, and $\chi(\omega)$ is the complex electric susceptibility. Since the dielectric permittivity $\mathbf{D}$ must obey the principle of causality, we have that the real and imaginary parts of the susceptibility $\chi(\omega)$, $\mathsf{Re}[\chi(\omega)]$, and $\mathsf{Im}[\chi(\omega)]$, respectively, are related by the Kramers-Kronig relations [27], [34], [35]:

$$\mathsf{Re}[\chi(\omega)] = \frac{2}{\pi}\mathcal{P}\int_0^{+\infty}\frac{\omega'\mathsf{Im}[\chi(\omega')]}{\omega'^2-\omega^2}d\omega' \tag{2}$$

$$\mathsf{Im}[\chi(\omega)] = -\frac{2\omega}{\pi}\mathcal{P}\int_0^{+\infty}\frac{\mathsf{Re}[\chi(\omega')]}{\omega'^2-\omega^2}d\omega' \tag{3}$$

where $\mathcal{P}$ denotes the Cauchy principal value. Jonscher derived his key insight from the experimental observations that an extensive range of solid dielectrics have a universal behavior in their susceptibility described by [34], [35]:

$$\chi(\omega) \propto \omega^{n-1} \quad n \in]0, 1[\tag{4}$$

where the exponent n governs the material frequency dispersion behavior. The result (4) in conjunction with the (2), (3), led Jonscher to conclude that the ratio between $\mathsf{Re}[\chi(\omega)]$, and $\mathsf{Im}[\chi(\omega)]$ must result independent from frequency and equal to:

$$\frac{\mathsf{Im}[\chi(\omega)]}{\mathsf{Re}[\chi(\omega)]} = \cot\left(\frac{n\pi}{2}\right). \tag{5}$$

Jonscher picked for the real part the following functional form:

$$\mathsf{Re}[\chi(\omega)] = \chi_r\left(\frac{\omega}{\omega_t}\right)^{n-1} \tag{6}$$

where ω_t is an arbitrary reference frequency and χ_r is the value of $\mathsf{Re}[\chi(\omega)]$ at this angular frequency, obtaining for $\chi(\omega)$ the following expression:

$$\chi(\omega) = \chi_r\left(\frac{\omega}{\omega_t}\right)^{n-1}\left[1 - i\cot\left(\frac{n\pi}{2}\right)\right] \tag{7}$$

from which the dielectric permittivity $\epsilon(\omega)$ reads as:

$$\epsilon(\omega) = \epsilon_0\chi_r\left(\frac{\omega}{\omega_t}\right)^{n-1}\left[1 - i\cot\left(\frac{n\pi}{2}\right)\right] + \varepsilon_\infty. \tag{8}$$

III. NONLINEAR OPTIMIZATION

A. PROBLEM FORMULATION

Ordinary concrete is a heterogeneous material, being an aggregate of sand, cement, and water [10], [11]. However, from the point of view of modeling its electromagnetic properties, concrete has always been treated as a homogeneous medium in the scientific literature because the inhomogeneities present in it have been considered small compared to the frequency of operation of the incident electromagnetic field [10], [12], [13]. In particular, since concrete is a porous material filled with an electrolyte solution, concrete has been modeled as a homogeneous and temporally dispersive electromagnetic material [10], [11], [12], [13]. Based on the above, given a series of m complex permittivity measurements $\boldsymbol{\epsilon}_M = \{\bar{\epsilon}(\omega_\alpha)\}_{\alpha=1}^m$ conducted on the concrete at hand, to obtain the Jonscher model (8) for the dielectric permittivity $\epsilon(\omega)$, it is necessary to evaluate the triplet of parameters $(n, \chi_r, \epsilon_\infty)$ related to it, solving the following NLSP [42]:

$$\min_{\boldsymbol{\theta}\in\mathbb{R}^3}\Phi(\boldsymbol{\theta}) = \|\boldsymbol{\epsilon}(\boldsymbol{\theta}) - \boldsymbol{\epsilon}_M\|_2 \tag{9}$$

where $\boldsymbol{\theta} = [n, \chi_r, \epsilon_\infty]^t$ is the vector of parameters, $\boldsymbol{\epsilon}(\boldsymbol{\theta})$ is the vector of model's predictions:

$$\begin{aligned}\boldsymbol{\epsilon}(\boldsymbol{\theta}) =& [\epsilon_0\chi_r\left(\frac{\omega_\alpha}{\omega_t}\right)^{n-1}\cdot \\ &\cdot\left[1 - i\cot\left(\frac{n\pi}{2}\right)\right] + \varepsilon_\infty]^t \;\; \alpha = 1, \ldots, m\end{aligned} \tag{10}$$

and $\Phi(\boldsymbol{\theta})$ is the residual between $\boldsymbol{\epsilon}(\boldsymbol{\theta})$ and the vector of the measured data $\boldsymbol{\epsilon}_M$ [31], [42].

B. ALGORITHMS

As stated in Section I, this study focuses on three standard algorithms for solving the NLSP (9) related to the Jonscher parametrization: i) the Levenberg-Marquardt (LM) method, which combines the Gauss-Newton algorithm with a trust-region approach and requires gradient information [41], ii) the BFGS algorithm, which is a quasi-Newton method that builds an approximation of the inverse Hessian from gradient evaluations [41], and iii) the Nelder-Mead algorithm, which is a derivative-free simplex algorithm, able to explore the parameter space through geometric transformations [41]. These methods are described in more detail in the following subsections.

1) NELDER-MEAD

The Nelder-Mead algorithm belongs to the class of direct search methods and operates on a simplex, a shape pattern consisting of $n+1$ vertices in the space of n dimensions [41], [50], [51], [52]. The idea behind the Nelder-Mead algorithm is to iteratively modify the shape of the simplex to navigate the search space. Each vertex corresponds to a candidate solution, and the algorithm modifies the simplex through geometric transformations such as reflection, expansion, contraction, and shrinkage to navigate the search space and minimize the objective function [50]. The algorithm does not require derivative information, which makes it particularly advantageous for problems in which the objective function is not smooth or complex to differentiate [51]. Instead, it relies on evaluations of the function at the vertices of the simplex and replaces the worst-performing vertex with a new candidate point to improve convergence to the optimal solution. Table (1) shows a pseudocode of the Nelder-Mead algorithm [50], [52].

Algorithm 1 Nelder-Mead Pseudocode

Input: Initial guess $\boldsymbol{\theta}_0$,**MaxIter**, tolerance τ
Output: Optimized parameters $\boldsymbol{\theta}^*$
Initialize simplex $S = \{\boldsymbol{\theta}^{(0)}, \boldsymbol{\theta}^{(1)}, \boldsymbol{\theta}^{(2)}, \boldsymbol{\theta}^{(3)}\}$ around $\boldsymbol{\theta}_0$
Evaluate $\Phi(\boldsymbol{\theta}^{(k)})$ for all $k = 0, 1, 2, 3$
for $t = 1$ to **Maximum iterations do**
  Order simplex: $\Phi(\boldsymbol{\theta}^{(0)}) \leq \Phi(\boldsymbol{\theta}^{(1)}) \leq \Phi(\boldsymbol{\theta}^{(2)}) \leq \Phi(\boldsymbol{\theta}^{(3)})$
  if $\|\Phi(\boldsymbol{\theta}^{(3)}) - \Phi(\boldsymbol{\theta}^{(0)})\| < \tau$ **then stop**
  end if
  Compute centroid $\boldsymbol{\theta}_c = \frac{1}{3}\sum_{k=0}^{2} \boldsymbol{\theta}^{(k)}$
  Reflection: $\boldsymbol{\theta}_r = \boldsymbol{\theta}_c + \alpha(\boldsymbol{\theta}_c - \boldsymbol{\theta}^{(3)})$
  if $\Phi(\boldsymbol{\theta}_r) < \Phi(\boldsymbol{\theta}^{(0)})$ **then**
    Expansion: $\boldsymbol{\theta}_e = \boldsymbol{\theta}_c + \gamma(\boldsymbol{\theta}_r - \boldsymbol{\theta}_c)$
    Replace $\boldsymbol{\theta}^{(3)}$ with $\arg\min(\Phi(\boldsymbol{\theta}_r), \Phi(\boldsymbol{\theta}_e))$
  else if $\Phi(\boldsymbol{\theta}_r) < \Phi(\boldsymbol{\theta}^{(2)})$ **then**
    Replace $\boldsymbol{\theta}^{(3)}$ with $\boldsymbol{\theta}_r$
  else
    Contraction: $\boldsymbol{\theta}_{con} = \boldsymbol{\theta}_c + \rho(\boldsymbol{\theta}^{(3)} - \boldsymbol{\theta}_c)$
    if $\Phi(\boldsymbol{\theta}_{con}) < \Phi(\boldsymbol{\theta}^{(3)})$ **then**
      Replace $\boldsymbol{\theta}^{(3)}$ with $\boldsymbol{\theta}_{con}$
    else
      Shrink: $\boldsymbol{\theta}^{(k)} = \boldsymbol{\theta}^{(0)} + \sigma(\boldsymbol{\theta}^{(k)} - \boldsymbol{\theta}^{(0)})$ for $k = 1, 2, 3$
    end if
  end if
end for
return $\boldsymbol{\theta}^* = \boldsymbol{\theta}^{(0)}$

2) BROYDEN-FLETCHER-GOLDFARB-SHANNO (BFGS) QUASI-NEWTON

The Broyden-Fletcher-Goldfarb-Shanno quasi-Newton algorithm (BFGS for short from now on) is an optimization method for unconstrained problems, fundamentally different from the derivative-free Nelder-Mead approach [41], [53], [54]. BFGS requires first-order derivatives to construct Hessian approximations, which are updated iteratively to improve the search direction, using gradient information and avoiding explicit computation of second-order derivatives, while Nelder-Mead operates without gradient information. BFGS achieves superlinear convergence for smooth objectives, outperforming Nelder-Mead's linear convergence [54]. The main advantages include faster convergence than gradient descent, robust performance in homogeneous optimization problems, and efficient memory utilization in large-scale environments (especially with the L-BFGS variant) [54]. However, BFGS requires the objective function to be differentiable and may have difficulties with highly nonlinear or noisy problems [53]. Table (2) shows a pseudocode of the BFGS algorithm [53], [54].

3) LEVENBERG-MARQUARDT

The Levenberg-Marquardt (LM) algorithm is an optimization technique that combines the second-order efficiency of

Algorithm 2 BFGS Quasi-Newton Pseudocode

Input: Initial guess $\boldsymbol{\theta}_0$, initial Hessian approximation $\boldsymbol{B}_0 = \boldsymbol{I} \in \mathbb{R}^{3\times 3}$, **MaxIter**,$N_{max}$, **Gradient tolerance** τ
Output: Optimized parameters $\boldsymbol{\theta}^*$
Compute initial gradient $\nabla\Phi(\boldsymbol{\theta}_0) = \left[\frac{\partial\Phi}{\partial\chi_r}, \frac{\partial\Phi}{\partial n}, \frac{\partial\Phi}{\partial\epsilon_\infty}\right]^\top$
for $t = 0$ to $N_{max} - 1$ **do**
  if $\|\nabla\Phi(\boldsymbol{\theta}_t)\|_2 < \tau$ **then stop**
  end if
  Compute search direction: $\boldsymbol{p}_t = -\boldsymbol{B}_t^{-1}\nabla\Phi(\boldsymbol{\theta}_t)$
  Perform line search: find $\alpha_t > 0$ minimizing $\Phi(\boldsymbol{\theta}_t + \alpha_t\boldsymbol{p}_t)$
  Update parameters: $\boldsymbol{\theta}_{t+1} = \boldsymbol{\theta}_t + \alpha_t\boldsymbol{p}_t$
  Compute gradient difference: $\boldsymbol{y}_t = \nabla\Phi(\boldsymbol{\theta}_{t+1}) - \nabla\Phi(\boldsymbol{\theta}_t)$
  Compute parameter difference: $\boldsymbol{s}_t = \boldsymbol{\theta}_{t+1} - \boldsymbol{\theta}_t$
  Update Hessian approximation:
$$\boldsymbol{B}_{t+1} = \boldsymbol{B}_t + \frac{\boldsymbol{y}_t\boldsymbol{y}_t^\top}{\boldsymbol{y}_t^\top\boldsymbol{s}_t} - \frac{\boldsymbol{B}_t\boldsymbol{s}_t(\boldsymbol{B}_t\boldsymbol{s}_t)^\top}{\boldsymbol{s}_t^\top\boldsymbol{B}_t\boldsymbol{s}_t}$$
end for
return $\boldsymbol{\theta}^* = \boldsymbol{\theta}_t$

Algorithm 3 Levenberg-Marquardt Pseudocode

Input: Initial guess $\boldsymbol{\theta}_0$, damping parameter $\lambda_0 > 0$, **OptimalityTolerance** τ, **MaxIter** N_{max}, scale factor $\nu > 1$
Output: Optimized parameters $\boldsymbol{\theta}^*$
Initialize $\boldsymbol{\theta} \leftarrow \boldsymbol{\theta}_0$, $\lambda \leftarrow \lambda_0$
Compute residual vector $\boldsymbol{r}(\boldsymbol{\theta}) = \boldsymbol{\epsilon}(\boldsymbol{\theta}) - \boldsymbol{\epsilon}_M \in \mathbb{R}^m$
Compute Jacobian $\boldsymbol{J} = \left[\frac{\partial\boldsymbol{\epsilon}}{\partial\chi_r}, \frac{\partial\boldsymbol{\epsilon}}{\partial n}, \frac{\partial\boldsymbol{\epsilon}}{\partial\epsilon_\infty}\right] \in \mathbb{R}^{m\times 3}$
for $t = 0$ to $N_{max} - 1$ **do**
  Compute gradient: $\nabla\Phi(\boldsymbol{\theta}) = 2\boldsymbol{J}^\top\boldsymbol{r}(\boldsymbol{\theta})$
  if $\|\nabla\Phi(\boldsymbol{\theta})\|_2 < \tau$ **then stop**
  end if
  Solve $(\boldsymbol{J}^\top\boldsymbol{J} + \lambda\cdot\mathrm{diag}(\boldsymbol{J}^\top\boldsymbol{J}))\boldsymbol{p} = -\boldsymbol{J}^\top\boldsymbol{r}(\boldsymbol{\theta})$
  Compute candidate: $\boldsymbol{\theta}_{new} = \boldsymbol{\theta} + \boldsymbol{p}$
  Compute new residual: $\boldsymbol{r}_{new} = \boldsymbol{\epsilon}(\boldsymbol{\theta}_{new}) - \boldsymbol{\epsilon}_M$
  Calculate ratio $\rho = \frac{\Phi(\boldsymbol{\theta}) - \Phi(\boldsymbol{\theta}_{new})}{\boldsymbol{p}^\top(\lambda\boldsymbol{p} + \boldsymbol{J}^\top\boldsymbol{r}(\boldsymbol{\theta}))}$
  if $\rho > 0$ **then**
    Accept step: $\boldsymbol{\theta} \leftarrow \boldsymbol{\theta}_{new}, \boldsymbol{r} \leftarrow \boldsymbol{r}_{new}$
    Update Jacobian $\boldsymbol{J}$ at $\boldsymbol{\theta}_{new}$
    Decrease damping: $\lambda \leftarrow \lambda/\nu$
  else
    Reject step: $\lambda \leftarrow \lambda\cdot\nu$
  end if
end for
return $\boldsymbol{\theta}^* = \boldsymbol{\theta}$

Gauss-Newton with the robustness of gradient descent [41], [55]. This duality contrasts with the derivative-free geometric operations of Nelder-Mead and the quasi-Newton approximations of BFGS [55], [56]. Where Nelder-Mead manipulates simplex vertices through reflection and contraction operations, and BFGS updates inverse Hessian estimates via secant conditions, LM explicitly exploits the least-squares structure through adaptive damping of its Jacobian matrix. The algorithm's damping parameter λ introduces a dynamic trade-off absent in both BFGS and Nelder-Mead: for large λ, LM mimics gradient descent, while small λ activates Gauss-Newton steps. This hybrid behavior enables faster convergence than Nelder-Mead's linear rate while avoiding BFGS's sensitivity to ill-conditioned Hessian approximations. Its hybrid nature allows it to move smoothly from exploration (high damping factor) to utilization (low damping factor), ensuring efficient convergence even in challenging optimization scenarios. Table (3) shows a pseudocode of the Levenberg-Marquardt algorithm [55], [56].

4) INITIAL GUESS

The choice of a good initial guess solution is well known to be a key factor relative to the convergence and quality of the solution calculated by a nonlinear optimization technique. When the parameter domain is known, common strategies for generating an initial guess include random sampling within the domain, Latin Hypercube Sampling, or grid search over a coarse mesh. These approaches can select one or multiple initial points and then evaluate the residual norm to choose the most promising candidate. Heuristic or expert-driven initialization is often used for problems with known physical meaning or structure. Alternatively, simple models (e.g., linear approximations or low-order Taylor expansions) can provide rough estimates. Nelder-Mead, being derivative-free, is often more tolerant of poor initial guesses, though it may converge slowly. BFGS and Levenberg-Marquardt, which use gradient and/or Jacobian information, generally benefit from better initial estimates to avoid convergence to local minima or saddle points. As stated in section II, the Jonscher model (8) requires the determination of three parameters, $(n, \chi_r, \epsilon_\infty)$, to be set for describing the complex dielectric permittivity $\epsilon(\omega)$ of an assigned material. Following the approach provided by the work [28], it is possible to analytically evaluate these coefficients by choosing arbitrarily two frequencies f_1 and f_2; after this choice, the exponent n of (8) is given by:

$$n = \frac{\mathsf{Log}(\mathsf{Im}[\epsilon_{meas}(2\pi f_1)]) - \mathsf{Log}(\mathsf{Im}[\epsilon_{meas}(2\pi f_2)]}{\mathsf{Log}(2\pi f_1) - \mathsf{Log}(2\pi f_2)} + 1 \tag{11}$$

where $\mathsf{Log}(\cdot)$ is the base 10 logarithm function. Next, fixing $\omega_t = 2\pi f_1$ the parameter χ_r can be determined as:

$$\chi_r = \frac{\mathsf{Re}[\epsilon_{meas}(2\pi f_2)] - \mathsf{Re}[\epsilon_{meas}(2\pi f_1)]}{\epsilon_0 \left[\left(\frac{f_2}{f_1}\right)^{n-1} - 1 \right]} \tag{12}$$

Finally, the parameter, ϵ_∞ can be computed by means of:

$$\epsilon_\infty = \mathsf{Re}[\epsilon_{meas}(2\pi f_1)] - \epsilon_0 \chi_r \tag{13}$$

The above triplet of values $(n, \chi_r, \epsilon_\infty)$ that we denote in what follows as P0, has be used as an initial guess θ_0 for the various nonlinear optimization algorithms discussed in sections III-B1, III-B2, and III-B3.

TABLE 1. Convergence criteria and tolerances for the Nelder-Mead, BFGS, and Levenberg-Marquardt optimization algorithms.

Algorithm	Parameter	Value
Nelder-Mead `fminsearch`	`TolFun`	10^{-4}
	`TolX`	10^{-4}
	`MaxIter`	200
	`MaxFunEvals`	600
BFGS `fminunc`	`TolFun / FunctionTolerance`	10^{-6}
	`TolX`	10^{-6}
	`MaxIter`	400
	`OptimalityTolerance`	10^{-6}
Levenberg-Marquardt `lsqnonlin`	`FunctionTolerance`	10^{-6}
	`StepTolerance`	10^{-6}
	`OptimalityTolerance`	10^{-6}

IV. NUMERICAL RESULTS

Since the result provided by an assigned nonlinear optimization procedure for solving an NLSP is highly dependent on the initial guess, noise, and its distribution in the data, for the analysis of the performance of the Nelder-Mead, BFGS, and Levenberg-Marquardt algorithms, we carried out a first phase of validation of their behavior using synthetic data, to isolate the factors influencing their performance and the quality of the computed solution. In contrast to real data, synthetic data allows complete control over the above factors, allowing us to identify why a procedure may or may not be effective. Afterward, in the second phase, we analyzed the performance of the selected algorithms on real data, thereby verifying whether the considerations made about their behavior in the first part of our study were confirmed. As already established in the section III-B4, we use eqs. (11), (12), and (13) to evaluate the initial guess P0 for each of the considered nonlinear optimization procedures. Furthermore, because P0 has been used in [28] and [29] directly as a Jonscher parametrization of the concrete permittivity, we have also compared its fitting ability with those of the final fitting solutions provided by the considered nonlinear optimization procedures to understand when and how P0 can be considered an optimal solution for Jonscher parameterization of the concrete at hand. All numerical experiments have been executed using the MATLAB R2023a© environment running on a machine based on Intel(R) Core(TM) i5-4570S CPU at 2.90GHz. The related simulation code has been implemented by exploiting the MATLAB built-in functions **fminsearch** for the Nelder-Mead method, **fminunc**, with the **quasi-newton** algorithm option, for the BFGS method, and **lsqnonlin** for the Levenberg-Marquardt method. For each of them, the settings employed have been the following: for the **fiminsearch** function, a termination tolerance on the function value, **TolFun**, and on the parameters, **TolX**, equal to 10^{-4}; a maximum number of iterations **MaxIter** and of function evaluation **MaxFunEvals** equal to 200 and 600, respectively. For the **fminunc** function the parameters **TolFun** and **TolX** have been selected equal to 10^{-6}; the parameter **MaxIter** has been selected equal to 400. The gradient evaluations have been performed internally via finite difference approximation

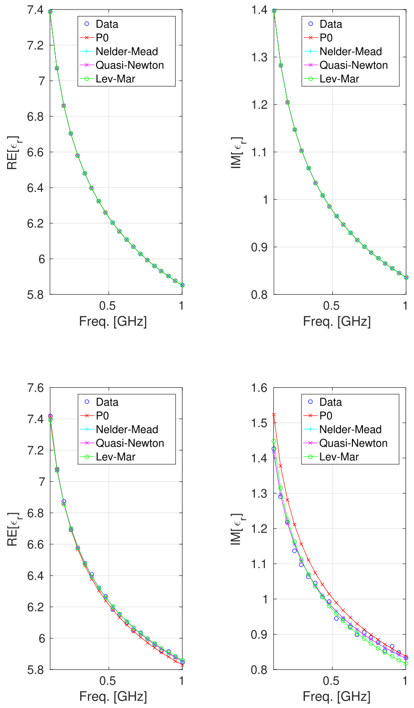

FIGURE 1. Jonscher fitting behavior obtained by Nelder-Mead, BFGS, and Levenberg-Marquardt nonlinear optimization procedures and by the analytic method P0, respectively, for the permittivity synthetic data generated by a Jonscher model with parameters $n = 0.78$, $\chi_r = 3.82$, and $\epsilon_\infty/\epsilon_0 = 3.57$. Top: noiseless data; mid: noisy data, $\sigma = 0.01$.

(as the Jacobian cannot be analytically provided in our case) with parameter OptimalityTolerance equal to 10^{-6}. The parameter FunctionTolerance has been selected equal to 10^{-6} (this parameter is formally equivalent to the TolFun parameter). Finally, for the lsqnonlin function the set of parameters FunctionTolerance, StepTolerance and OptimalityTolerance have been selected equal to 10^{-6}. Table (1) summarizes all the selected convergence criteria and tolerances for the considered procedures.

To quantify and compare the performance of the various fitting results the following metrics has been considered: the means square error (MSE):

$$\mathrm{MSE} = \frac{1}{m}\sum_{\alpha=1}^{m} |\epsilon(\theta)_\alpha - \bar{\epsilon}_\alpha|^2 \tag{14}$$

the means absolute error (MAE):

$$\mathrm{MAE} = \frac{1}{m}\sum_{\alpha=1}^{m} |\epsilon(\theta)_\alpha - \bar{\epsilon}_\alpha| \tag{15}$$

and the mean absolute percentage error (MAPE):

$$\mathrm{MAPE} = \frac{1}{m}\sum_{\alpha=1}^{m} \left|\frac{\epsilon(\theta)_\alpha - \bar{\epsilon}_\alpha}{\bar{\epsilon}_\alpha}\right| \% \tag{16}$$

A. SYNTHETIC DATA

All the abovementioned procedures have been tested using noiseless and noisy artificially generated data. The noise we added to the real and imaginary parts of the noiseless complex permittivity was uncorrelated and normally distributed, with mean values $\mu_d = 0$ and standard deviations of $\sigma = 0.01$, $\sigma = 0.05$, and $\sigma = 0.1$, respectively. These noise values, which can be considered representative of low,

TABLE 2. Jonscher parameters from Nelder-Mead, BFGS, and Levenberg-Marquardt non-linear optimization procedures and by the analytic method P0 for the noiseless and noisy synthetic Jonscher concrete permittivity model data.

noiseless	n	χ_r	$\epsilon_\infty/\epsilon_0$
P0	0.78	3.82	3.57
Nelder-Mead	0.78	3.82	3.57
BFGS	0.78	3.82	3.57
Lev-Mar	0.78	3.82	3.57
$\mu_d = 0.0$, $\sigma = 0.01$	n	χ_r	$\epsilon_\infty/\epsilon_0$
P0	0.74	3.52	3.89
Nelder-Mead	0.769	3.73	3.66
BFGS	0.769	3.73	3.66
Lev-Mar	0.751	3.52	3.88
$\mu_d = 0.0$, $\sigma = 0.05$	n	χ_r	$\epsilon_\infty/\epsilon_0$
P0	0.748	3.56	3.83
Nelder-Mead	0.782	3.83	3.53
BFGS	0.782	3.83	3.53
Lev-Mar	0.761	3.55	3.81
$\mu_d = 0.0$, $\sigma = 0.1$	n	χ_r	$\epsilon_\infty/\epsilon_0$
PO	0.401	2.43	5.02
Nelder-Mead	0.749	3.52	3.88
Quasi-Newton	0.749	3.52	3.88
Lev-Mar	0.63	2.55	4.82

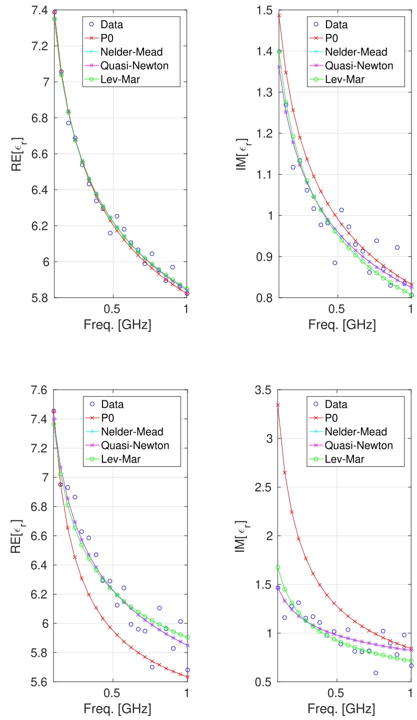

FIGURE 2. Jonscher fitting behavior obtained by Nelder-Mead, BFGS, and Levenberg-Marquardt nonlinear optimization procedures and by the analytic method P0, respectively, for the permittivity synthetic data generated by a Jonscher model with parameters $n = 0.78$, $\chi_r = 3.82$, and $\epsilon_\infty/\epsilon_0 = 3.57$. Top: noisy data, $\sigma = 0.05$, bottom: noisy data, $\sigma = 0.1$.

TABLE 3. MSE, MAE, MAPE, and CPU Time for the Jonscher parametrization obtained by Nelder-Mead, BFGS, and Levenberg-Marquardt nonlinear optimization procedures and by the analytic method P0 for the synthetic Jonscher concrete permittivity model data: noiseless data.

	P0	Nelder Mead	Quasi	Levenberg Marquardt
MSE	$5.33e-16$	$5.33e-16$	$5.33e-16$	$5.33e-16$
MSE[Re]	$3.29e-16$	$3.29e-16$	$3.29e-16$	$3.29e-16$
MSE[Im]	$4.19e-16$	$4.19e-16$	$4.19e-16$	$4.19e-16$
MAE	$2.37e-15$	$1.07e-14$	$1.07e-14$	$1.07e-14$
MAE[Re]	$1.29e-15$	$2.37e-15$	$2.37e-15$	$2.37e-15$
MAE[Im]	$1.87e-15$	$1.29e-15$	$1.29e-15$	$1.29e-15$
MAPE	$3.73e-14$	$1.87e-15$	$1.87e-15$	$1.87e-15$
MAPE(Re)	$2.09e-14$	$3.73e-14$	$3.73e-14$	$3.73e-14$
MAPE(Im)	$1.88e-13$	$2.09e-14$	$2.09e-14$	$2.09e-14$
CPU-Time (sec.)	–	0.00528	0.00811	0.00377

TABLE 4. MSE, MAE, MAPE, and CPU Time for the Jonscher parametrization obtained by Nelder-Mead, BFGS, and Levenberg-Marquardt nonlinear optimization procedures and by the analytic method P0 for the synthetic Jonscher concrete permittivity model data: noisy data, $\sigma = 0.01$.

	P0	Nelder Mead	BFGS	Levenberg Marquardt
MSE	0.0109	0.00322	0.00322	0.00436
MSE[Re]	0.00429	0.00236	0.00236	0.00257
MSE[Im]	0.00997	0.00219	0.00219	0.00352
MAE	0.0435	0.0644	0.0644	0.0873
MAE[Re]	0.0161	0.0124	0.0124	0.0179
MAE[Im]	0.0349	0.00838	0.00838	0.00892
MAPE	0.663	0.00837	0.00837	0.0135
MAPE(Re)	0.262	0.192	0.192	0.28
MAPE(Im)	3.19	0.131	0.131	0.14
CPU-Time (sec.)	–	0.0046	0.0115	0.0348

TABLE 5. MSE, MAE, MAPE, and CPU Time for the Jonscher parametrization obtained by Nelder-Mead, BFGS, and Levenberg-Marquardt nonlinear optimization procedures and by the analytic method P0 for the synthetic Jonscher concrete permittivity model data: noisy data, $\sigma = 0.05$.

	P0	Nelder Mead	BFGS	Levenberg Marquardt
MSE	0.0175	0.0129	0.0129	0.0134
MSE[Re]	0.00992	0.00915	0.00915	0.00889
MSE[Im]	0.0145	0.00914	0.00914	0.01
MAE	0.069	0.259	0.259	0.268
MAE[Re]	0.0323	0.0464	0.0464	0.0489
MAE[Im]	0.0534	0.0328	0.0328	0.0325
MAPE	1.07	0.0327	0.0327	0.0331
MAPE(Re)	0.521	0.73	0.73	0.774
MAPE(Im)	5.26	0.523	0.523	0.518
CPU-Time (sec.)	–	0.00388	0.00874	0.0335

moderate, and high noise scenarios [16], have been taken into account with the aim of evaluating the behavior of all the methods we considered as the noise level worsen. Numerical experiments in the presence of noise have been conducted 30 times, and what is reported in what follows refers to the average behavior for each method. The first case we considered was that of artificially generated data by a Jonscher model with parameters $n = 0.78$, $\chi_r = 3.82$, and $\epsilon_\infty/\epsilon_0 = 3.57$ (an artificial model that can be considered representative of concrete with a low moisture content level [31]). The data has been generated in the frequency range [0.1, 1] GHz. To compute the initial guess P0, we have selected $f_1 = 0.1$ GHz and $f_2 = 0.145$ GHz, checking that, as a result of this choice, the triple of Jonscher's parameters was consistent (i.e., all parameters were positive, with $n \in]0, 1[$). The number of generated samples, m, was equal to 20. Figures (1), (2) show the fitting accuracy of the various Jonscher parameterizations obtained by the analytical method, P0, and by solving the NLSP (9) with the Nelder-Mead, BFGS quasi-Newton, and Levenberg-Marquardt methods, respectively. The results reported at

TABLE 6. MSE, MAE, MAPE, and CPU Time for the Jonscher parametrization obtained by Nelder-Mead, BFGS, and Levenberg-Marquardt nonlinear optimization procedures and by the analytic method P0 for the synthetic Jonscher concrete permittivity model data: noisy data, $\sigma = 0.1$.

	P0	Nelder Mead	BFGS	Levenberg Marquardt
MSE	0.159	0.0369	0.0369	0.0428
MSE[Re]	0.0601	0.0264	0.0264	0.0297
MSE[Im]	0.147	0.0257	0.0257	0.0309
MAE	0.571	0.738	0.738	0.857
MAE[Re]	0.234	0.141	0.141	0.17
MAE[Im]	0.465	0.102	0.102	0.113
MAPE	8.58	0.0948	0.0948	0.105
MAPE(Re)	3.71	2.26	2.26	2.68
MAPE(Im)	42.8	1.65	1.65	1.82
CPU-Time (sec.)	–	0.0213	0.0528	0.0567

TABLE 7. Jonscher parameters from Nelder-Mead, BFGS, and Levenberg-Marquardt non-linear optimization procedures and by the analytic method P0 for the noiseless and noisy synthetic Debye concrete permittivity model data, MC=2.8%.

noiseless	n	χ_r	$\epsilon_\infty/\epsilon_0$
P0	0.32	0.78	5.13
Nelder-Mead	0.219	0.337	5.45
BFGS	0.219	0.337	5.45
Lev-Mar	0.221	0.339	5.45
$\mu_d = 0.0$ $\sigma = 0.01$	n	χ_r	$\epsilon_\infty/\epsilon_0$
P0	0.297	0.798	5.13
Nelder-Mead	0.219	0.337	5.45
BFGS	0.219	0.337	5.45
Lev-Mar	0.22	0.339	5.45
$\mu_d = 0.0$ $\sigma = 0.05$	n	χ_r	$\epsilon_\infty/\epsilon_0$
P0	0.512	1.61	4.3
Nelder-Mead	0.203	0.318	5.44
BFGS	0.203	0.318	5.44
Lev-Mar	0.545	0.794	5.16
$\mu_d = 0.0$ $\sigma = 0.1$	n	χ_r	$\epsilon_\infty/\epsilon_0$
PO	0.646	1.51	4.39
Nelder-Mead	0.219	0.331	5.45
Quasi-Newton	0.219	0.331	5.45
Lev-Mar	0.413	0.605	5.27

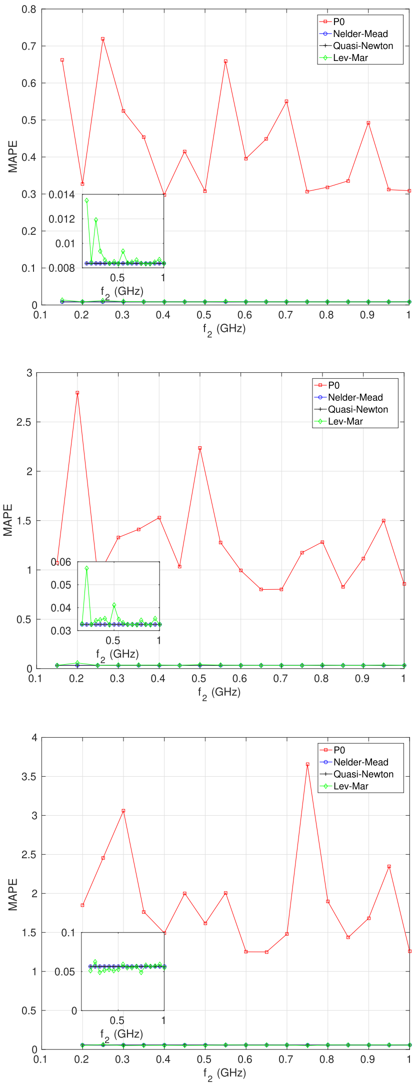

FIGURE 3. MAPE for the Jonscher parametrizations obtained by Nelder-Mead, BFGS, and Levenberg-Marquardt nonlinear optimization procedures as a function of the frequency f_2 for the synthetic Jonscher data. Top: $\sigma = 0.01$; mid: $\sigma = 0.05$; bottom: $\sigma = 0.1$.

the top of Figure (1) in Table (2) and (3) show as in the case of noiseless data, the fitting result provided by all the considered approaches and their related metrics are the same and excellent in assumed values (as it was expected to be, due to the particularity of the considered data).

For the case of noisy data, the behavior of the various methods begins to differ, as can be observed by the results reported in the the bottom of Figure (1) and in Figure (2). The fitting of the analytic solution P0 yields poor metrics in terms of MAPE for the imaginary part of the complex permittivity with values of $\approx$ 3% for $\sigma = 0.01$, $\approx$ 5% for $\sigma = 0.05$, and $\approx$ 43% for $\sigma = 0.1$. In contrast, all nonlinear optimization methods provide a good fit to both the real and the imaginary parts of the complex permittivity data. More precisely, analyzing the results shown by Tables (2), (3), (4), (5), and (6) it can be seen that the Nelder-Mead

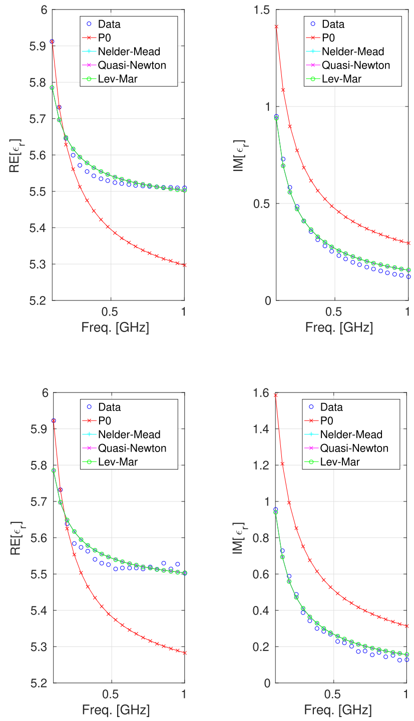

FIGURE 4. Jonscher fitting behavior obtained by Nelder-Mead, BFGS, and Levenberg-Marquardt nonlinear optimization procedures, and by the analytic method P0 for the synthetic permittivity data generated by a Debye concrete model with MC=2.8%. Top: noiseless data; bottom: noisy data $\sigma = 0.01$.

TABLE 8. MSE, MAE, MAPE, and CPU Time for the Jonscher parametrization obtained by Nelder-Mead, BFGS, and Levenberg-Marquardt nonlinear optimization procedures, and by the analytic method P0 for the synthetic Debye concrete permittivity model data, MC=2.8%: noiseless data.

	P0	Nelder Mead	BFGS	Levenberg Marquardt
MSE	0.0648	0.00924	0.00924	0.00924
MSE[Re]	0.0322	0.00717	0.00717	0.00713
MSE[Im]	0.0563	0.00582	0.00582	0.00588
MAE	0.286	0.185	0.185	0.185
MAE[Re]	0.126	0.035	0.035	0.0351
MAE[Im]	0.242	0.0177	0.0177	0.0177
MAPE	5.12	0.0241	0.0241	0.0243
MAPE(Re)	2.28	0.621	0.621	0.623
MAPE(Im)	96.2	0.312	0.312	0.311
CPU-Time (sec.)	–	0.0042	0.00745	0.0332

and BFGS methods are equivalent in term of fitting metrics (MSE$\leq$ 0.04, MAE$\leq$ 0.8, MAPE$\leq$ 0.095%) giving the same Jonscher parameterization for all the considered noise level, while the results provided by the Levenberg-Marquardt method are slightly different. In conclusion, for this case, all nonlinear optimization procedures are robust, i.e., they are able to provide a solution capable of good data fitting also in case of a high noise level scenario ($\sigma = 0.1$) with a MAPE consistently lower than 3%.

Concerning evaluating the efficiency of the considered procedures among the various criteria adopted in literature

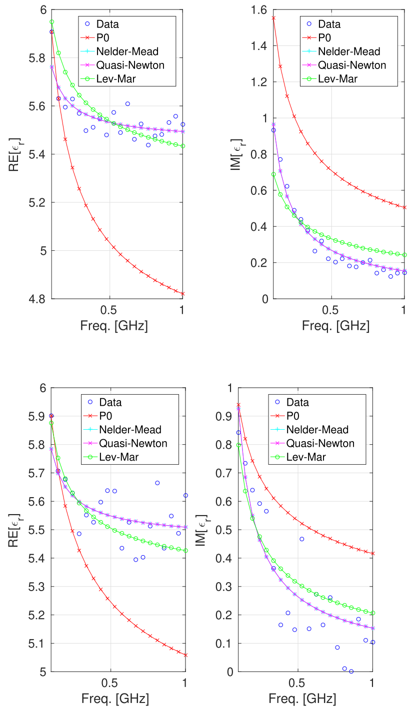

FIGURE 5. Jonscher fitting behavior obtained by Nelder-Mead, BFGS, and Levenberg-Marquardt nonlinear optimization procedures, and by the analytic method P0 for the synthetic permittivity data generated by a Debye concrete model with MC=2.8%. Top: noisy data $\sigma = 0.05$, bottom: noisy data $\sigma = 0.1$.

TABLE 9. MSE, MAE, MAPE, and CPU Time for the Jonscher parametrization obtained by Nelder-Mead, BFGS, and Levenberg-Marquardt nonlinear optimization procedures, and by the analytic method P0 for the synthetic Debye concrete permittivity model data, MC=2.8%: noisy data, $\sigma = 0.01$.

	P0	Nelder Mead	BFGS	Levenberg Marquardt
MSE	0.078	0.01	0.01	0.01
MSE[Re]	0.035	0.0081	0.0081	0.00806
MSE[Im]	0.0697	0.00588	0.00588	0.00593
MAE	0.339	0.2	0.2	0.2
MAE[Re]	0.136	0.0372	0.0372	0.0374
MAE[Im]	0.292	0.0224	0.0224	0.0223
MAPE	6.05	0.0248	0.0248	0.0251
MAPE(Re)	2.47	0.66	0.66	0.663
MAPE(Im)	111	0.394	0.394	0.393
CPU-Time (sec.)	–	0.0045	0.00725	0.0337

(that is, the number of iterations, the number of function evaluations) in what follows, we have considered the CPU Time involved in the resolution of (9) since, as explained in the section III-B, the various methods base their operation on principles of operation that are not related to each other [57], [58].

Although the CPU times involved in the various numerical simulations are negligible in absolute value (also considering the dataset sizes), the results in Tables (3), (4), (5), and (6) based on 30 repeated experiments, indicate that the Levenberg-Marquardt was the fastest only in the noiseless

TABLE 10. MSE, MAE, MAPE, and CPU Time for the Jonscher parametrization obtained by Nelder-Mead, BFGS, and Levenberg-Marquardt nonlinear optimization procedures, and by the analytic method P0 for the synthetic Debye concrete permittivity model data, MC=2.8%: noisy data, $\sigma = 0.05$.

	P0	Nelder Mead	BFGS	Levenberg Marquardt
MSE	0.152	0.0149	0.0149	0.0316
MSE[Re]	0.112	0.0123	0.0123	0.0186
MSE[Im]	0.103	0.00833	0.00833	0.0255
MAE	0.675	0.298	0.298	0.631
MAE[Re]	0.452	0.0587	0.0587	0.13
MAE[Im]	0.456	0.0454	0.0454	0.0697
MAPE	12.1	0.0319	0.0319	0.101
MAPE(Re)	8.19	1.05	1.05	2.32
MAPE(Im)	190	0.813	0.813	1.25
CPU-Time (sec.)	–	0.00502	0.00953	0.035

TABLE 11. MSE, MAE, MAPE, and CPU Time for the Jonscher parametrization obtained by Nelder-Mead, BFGS, and Levenberg-Marquardt nonlinear optimization procedures, and by the analytic method P0 for the synthetic Debye concrete permittivity model data, MC=2.8%: noisy data, $\sigma = 0.1$.

	P0	Nelder Mead	BFGS	Levenberg Marquardt
MSE	0.0966	0.0307	0.0307	0.0359
MSE[Re]	0.0721	0.0183	0.0183	0.0208
MSE[Im]	0.0643	0.0247	0.0247	0.0292
MAE	0.391	0.614	0.614	0.718
MAE[Re]	0.278	0.124	0.124	0.144
MAE[Im]	0.257	0.0669	0.0669	0.0715
MAPE	7.04	0.0954	0.0954	0.114
MAPE(Re)	5	2.23	2.23	2.59
MAPE(Im)	$2.28e+03$	1.2	1.2	1.28
CPU-Time (sec.)	–	0.0144	0.0476	0.0795

case. In the presence of low and moderate noise levels ($\sigma = 0.01$ and $\sigma = 0.05$), Nelder-Mead and BFGS consistently outperformed it in terms of CPU Time: when $\sigma = 0.01$, the average execution time of Nelder-Mead was 7.5 times lower, and that of BFGS was 3.02 times lower; for $\sigma = 0.05$, these factors increased to 8.6$\times$ and 3.77$\times$, respectively. Quite different is the behavior of the considered methods in terms of this parameter in the presence of a high noise level ($\sigma = 0.1$): in this case, the average CPU Time of the Levenber-Marquardt method was approximately equal to that of BFGS. At the same time, albeit worsening in its performances, the Nelder-Mead method remained the fastest (as expected), with a speedup factor of approximately 2.66 times over the Levenberg-Marquardt algorithm.

Figure (3) shows the trend of the MAPE of the analytical solution P0 as a function of the frequency f_2 used for its determination, for all the noise levels considered in our study (f_1 has been deemed fixed and equal to 0.1GHz). We note that this metric results erratic in its functional dependence on the choice of frequency f_2 used to calculate P0. The range of assumed values increased as the noise in the data increased; it remained less than 3% (a value that can be considered

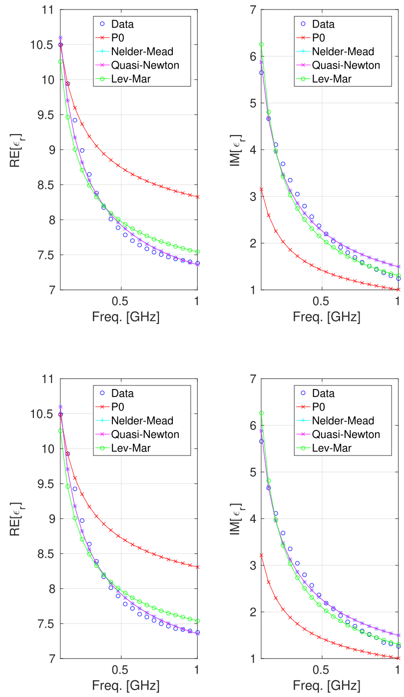

FIGURE 6. Jonscher fitting behavior obtained by Nelder-Mead, BFGS, and Levenberg-Marquardt nonlinear optimization procedures, and by the analytic method P0 for the synthetic permittivity data generated by a Debye concrete model with MC=9.3%. Top: noiseless data; mid: noisy data $\sigma = 0.01$, bottom: noisy data $\sigma = 0.05$.

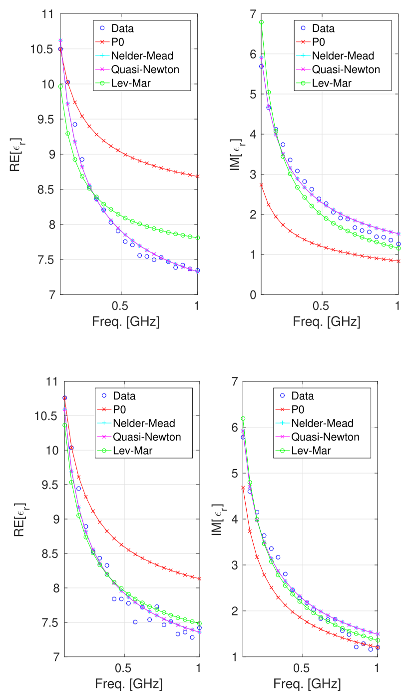

FIGURE 7. Jonscher fitting behavior obtained by Nelder-Mead, BFGS, and Levenberg-Marquardt nonlinear optimization procedures, and by the analytic method P0 for the synthetic permittivity data generated by a Debye concrete model with MC=9.3%. Top: noiseless data; mid: noisy data $\sigma = 0.05$, bottom: noisy data $\sigma = 0.1$.

acceptable for practical applications) up to the moderate noise threshold of sigma=0.05 and then exceeded this limit in the case of a high noise threshold of sigma=0.1, albeit

TABLE 12. Jonscher parameters from Nelder-Mead, BFGS, and Levenberg-Marquardt non-linear optimization procedures and by the analytic method P0 for the noiseless and noisy synthetic Debye concrete permittivity model data, MC=9.3%.

noiseless	n	χ_r	$\epsilon_\infty/\epsilon_0$
P0	0.503	3.18	7.32
Nelder-Mead	0.405	4.35	6.25
BFGS	0.405	4.35	6.25
Lev-Mar	0.319	3.43	6.83
$\mu_d = 0.0$ $\sigma = 0.01$	n	χ_r	$\epsilon_\infty/\epsilon_0$
P0	0.497	3.18	7.31
Nelder-Mead	0.405	4.35	6.25
BFGS	0.405	4.35	6.25
Lev-Mar	0.319	3.43	6.83
$\mu_d = 0.0$ $\sigma = 0.05$	n	χ_r	$\epsilon_\infty/\epsilon_0$
P0	0.486	2.62	7.88
Nelder-Mead	0.41	4.44	6.19
BFGS	0.41	4.44	6.19
Lev-Mar	0.233	2.6	7.37
$\mu_d = 0.0$ $\sigma = 0.1$	n	χ_r	$\epsilon_\infty/\epsilon_0$
PO	0.411	3.53	7.23
Nelder-Mead	0.401	4.32	6.27
Quasi-Newton	0.401	4.32	6.27
Lev-Mar	0.342	3.69	6.67

TABLE 13. MSE, MAE, MAPE, and CPU Time for the Jonscher parametrization obtained by Nelder-Mead, BFGS, and Levenberg-Marquardt nonlinear optimization procedures, and by the analytic method P0 for the synthetic Debye concrete permittivity model data, MC=9.3%: noiseless data.

	P0	Nelder Mead	BFGS	Levenberg Marquardt
MSE	0.316	0.0434	0.0434	0.0684
MSE[Re]	0.181	0.0227	0.0227	0.0481
MSE[Im]	0.259	0.037	0.037	0.0487
MAE	1.36	0.868	0.868	1.37
MAE[Re]	0.741	0.184	0.184	0.279
MAE[Im]	0.964	0.0774	0.0774	0.189
MAPE	15.6	0.147	0.147	0.164
MAPE(Re)	9.59	2.14	2.14	3.13
MAPE(Im)	34.9	0.902	0.902	2.28
CPU-Time (sec.)	—	0.00427	0.00626	0.033

only slightly. In the same figure, we also plotted the MAPE trend of the fitting solution obtained from each optimization method as a function of the frequency f_2 used to evaluate the initial guess P0. As it can be observed, the Nelder-Mead and BFGS provided fitting is practically insensitive, in terms of MAPE, by its choice. On the contrary, the behavior of the Levenberg-Marquardt method results sensitive to the choice of the initial guess P0, albeit the MAPE values are more than optimal for every noise level (less than 0.2%).

As a more complex test, we analyzed the performance of the above methods using artificial complex permittivity data generated by the following Debye model:

$$\epsilon_D(\omega) = \left(\epsilon_\infty + \frac{\epsilon_{stat} - \epsilon_\infty}{1 + \omega^2\tau^2}\right) - j\left(\frac{\omega\tau[\epsilon_{stat} - \epsilon_\infty]}{1 + \omega^2\tau^2} + \frac{\sigma_{dc}}{\omega\epsilon_0}\right) \quad (17)$$

TABLE 14. MSE, MAE, MAPE, and CPU Time for the Jonscher parametrization obtained by Nelder-Mead, BFGS, and Levenberg-Marquardt nonlinear optimization procedures, and by the analytic method P0 for the synthetic Debye concrete permittivity model data, MC=9.3%: noisy data, $\sigma = 0.01$.

	P0	Nelder Mead	BFGS	Levenberg Marquardt
MSE	0.31	0.0427	0.0427	0.068
MSE[Re]	0.177	0.022	0.022	0.0475
MSE[Im]	0.255	0.0366	0.0366	0.0487
MAE	1.33	0.854	0.854	1.36
MAE[Re]	0.725	0.18	0.18	0.278
MAE[Im]	0.951	0.0756	0.0756	0.187
MAPE	15.3	0.144	0.144	0.164
MAPE(Re)	9.38	2.1	2.1	3.13
MAPE(Im)	34.4	0.881	0.881	2.26
CPU-Time (sec.)	–	0.00417	0.00684	0.0337

TABLE 15. MSE, MAE, MAPE, and CPU Time for the Jonscher parametrization obtained by Nelder-Mead, BFGS, and Levenberg-Marquardt nonlinear optimization procedures, and by the analytic method P0 for the synthetic Debye concrete permittivity model data, MC=9.3%: noisy data, $\sigma = 0.05$.

	P0	Nelder Mead	BFGS	Levenberg Marquardt
MSE	0.402	0.0442	0.0442	0.122
MSE[Re]	0.247	0.0243	0.0243	0.0894
MSE[Im]	0.317	0.0368	0.0368	0.0824
MAE	1.75	0.883	0.883	2.43
MAE[Re]	1.02	0.186	0.186	0.51
MAE[Im]	1.23	0.0738	0.0738	0.359
MAPE	20.3	0.15	0.15	0.301
MAPE(Re)	13.2	2.17	2.17	5.91
MAPE(Im)	45.8	0.854	0.854	4.45
CPU-Time (sec.)	–	0.00467	0.00739	0.0336

TABLE 16. MSE, MAE, MAPE, and CPU Time for the Jonscher parametrization obtained by Nelder-Mead, BFGS, and Levenberg-Marquardt nonlinear optimization procedures, and by the analytic method P0 for the synthetic Debye concrete permittivity model data, MC=9.3%: noisy data, $\sigma = 0.1$.

	P0	Nelder Mead	BFGS	Levenberg Marquardt
MSE	0.201	0.0576	0.0576	0.0683
MSE[Re]	0.155	0.0346	0.0346	0.0515
MSE[Im]	0.129	0.0461	0.0461	0.0448
MAE	0.894	1.15	1.15	1.37
MAE[Re]	0.634	0.241	0.241	0.275
MAE[Im]	0.46	0.126	0.126	0.193
MAPE	10.6	0.169	0.169	0.169
MAPE(Re)	8.22	2.87	2.87	3.14
MAPE(Im)	15.9	1.52	1.52	2.31
CPU-Time (sec.)	–	0.00401	0.0063	0.0337

whose coefficients $\epsilon_{stat}, \epsilon_\infty \tau, \sigma_{dc}$, reported in Table (1) of [29] were derived from experimental measurements on a concrete made of sand and gravel aggregate with maximum sizes of 10 mm and Ordinary Portland cement [28], [29]. For our numerical simulations, we considered three different levels of moisture content: 2.8%, 9.3% and 12%, respectively.

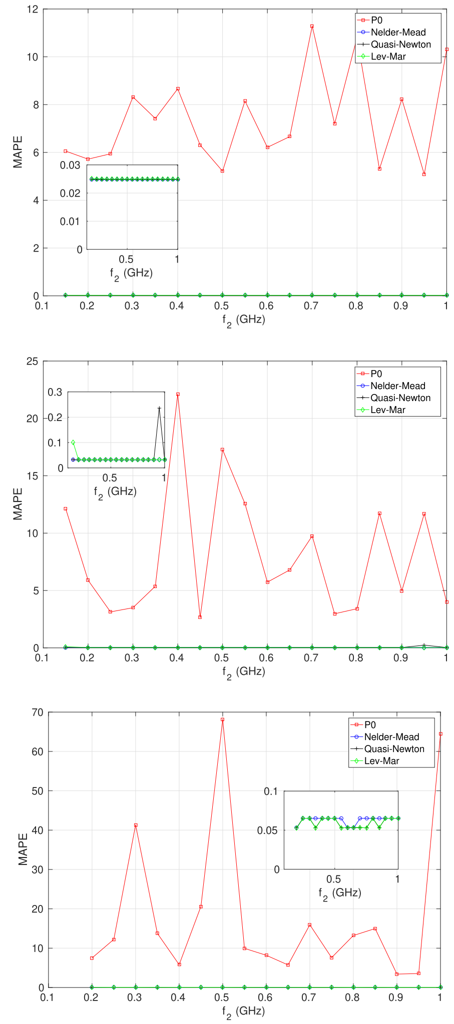

FIGURE 8. MAPE for the Jonscher parametrizations obtained by Nelder-Mead, BFGS, and Levenberg-Marquardt nonlinear optimization procedures as a function of the frequency f_2 for the Debye concrete model with MC=2.8%. Top: $\sigma = 0.01$; mid:$\sigma = 0.05$; bottom: σ : 0.1.

We made this choice to understand the influence of MC level on the quality of fitting provided by the considered procedures. For the numerical simulations conducted using this type of synthetic data, the range of frequencies considered, the number of samples, and the frequencies f_1 and f_2 employed for the calculation of P0 were the same as those used previously, constantly checking the consistency of the parameters $(n, \chi_r, \epsilon_\infty/\epsilon_0)$ constituting the initial guess P0.

In the case of the Debye concrete model with MC $=$ 2.8%, we can note from the analysis of the Tables (7), (8), (9), (10), (11) and Figures (4), (5) that quality of fitting solution provided by the Nelder-Mead, BFGS, and Levenberg-Marquardt methods was practically the same in the case of noiseless data and very similar in the case of noisy data with a noise level $\sigma = 0.01$. In this last case, all metrics took values no greater than the fraction of a unit (MSE$\leq$ 0.01, MAE$\leq$ 0.2), even percent (MAPE$\leq$ 0.3%) indicating very good fitting with the data for all methods used. For the case of

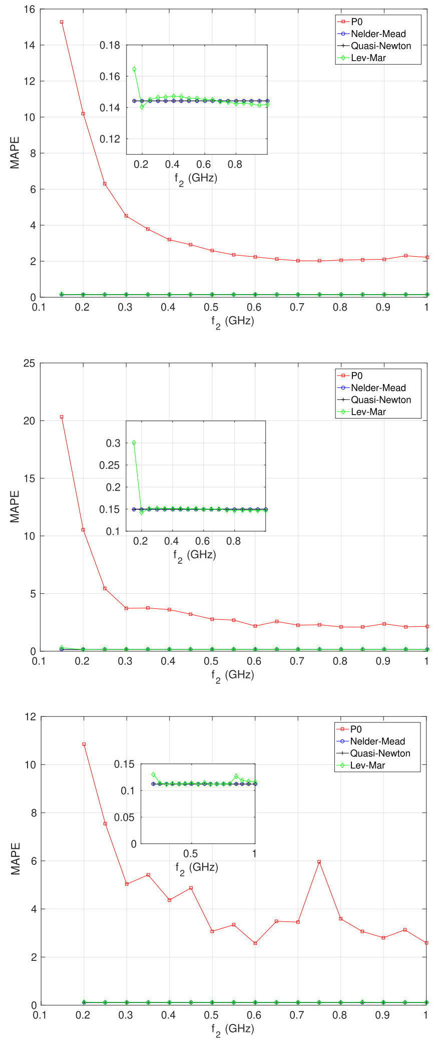

FIGURE 9. MAPE for the Jonscher parametrizations obtained by Nelder-Mead, BFGS, and Levenberg-Marquardt nonlinear optimization procedures as a function of the frequency f_2 for the Debye concrete model with MC=9.3%. Top: $\sigma = 0.01$; mid:$\sigma = 0.05$; bottom: σ : 0.1.

data corrupted with a noise level $\sigma = 0.05$, the quality of the fitting provided by the Levenberg-Marquardt method slightly worsened, especially in terms of MAPE referred to the real and the imaginary part of the data, compared with those given by the Nelder-Mead and the BFGS methods, assuming values in any case not exceeding 1.5%. Still, it is possible to consider that the methods provide a parameterization capable of suitable fitting with the data. On the contrary, the P0 solution provides a parameterization that is suitable only for noiseless data, becoming already unacceptable for data with a low noise level (MAPE(Im)$>$ 100%). At last, in the case of high noise level ($\sigma = 0.1$), taking into account the substantial deterioration in the error metrics considered, the qualitative assessments remain precisely the same for all methods examined.

Concerning the evaluation of the efficiency expressed in terms of CPU Time, the results shown in Tables (8), (9), (10), and (11) confirm what has already been observed in the

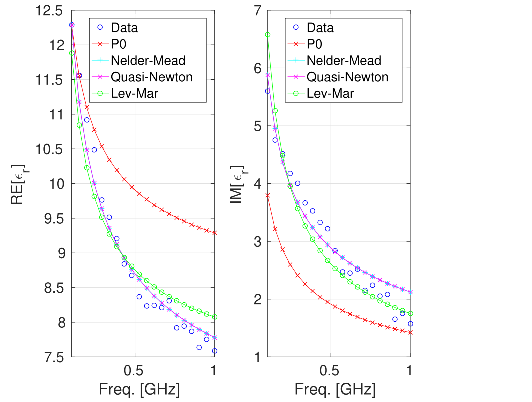

FIGURE 10. Jonscher fitting behavior obtained by Nelder-Mead, BFGS, and Levenberg-Marquardt nonlinear optimization procedures and by the analytic method P0 for the synthetic permittivity data generated by a Debye concrete model with MC=12%. Noisy data $\sigma = 0.1$.

previous case, i.e., Nelder-Mead and BFGS are always fastest than Levenberg-Marquardt in term of this parameter in any considered case, although this advantage worsen in the case of high noise level ($\sigma = 0.1$).

In the case of concrete with MC = 9.3%, from the results reported in Figures (6), (7), and Tables (12), (13), (14), (15), and (16) we can note that the fitting quality provided by the Nelder-Mead and BFGS methods resulted, as expected, in a degradation as noise increases, although the qualitative trend of the data is captured by the fitting. This behavior is quantified by the employed error metrics when compared to those of the concrete with MC = 2.8%. Regarding the Levenberg-Marquardt method, we observe that it suffers from a worse degradation of its performance compared to those offered by the other two methods, especially in cases of higher noise. For all the cases above considered, the analysis of MSE, MAE, and MAPE related to the real and imaginary part of the complex permittivity reveals that the quality of the fitting is better on the imaginary part than the real part of the permittivity. About the CPU Time, there is nothing new from what was previously stated, as clearly shown by the data reported in Tables (13), (14), (15), and (16) concerning this parameter.

Figures (8), (9) show the behavior of the MAPE related to the fitting solution computed by the Nelder-Mead, BFGS quasi-Newton, and Levenberg-Marquardt algorithms as a function of the frequency f_2 used to evaluate the initial guess solution P0, and of P0 itself, for the MC levels of 2.8% and 9.3%, respectively. It can be noticed as for the case of MC= 2.8%, the MAPE varies erratically for P0. In contrast, for the case of MC= 9.3%, the overall trend of the MAPE is downward sloping as the frequency increases. Decidedly less erratic is the behavior of MAPE related to the fitting obtained from the three nonlinear optimization techniques examined: the Nelder-Mead is the more stable among the selected methods, and the MAPE metric of its solution is close independent of the quality, in terms of MAPE, of the initial guess P0. On the contrary, both the BFGS and Levenberg-Marquardt techniques result in sensible behavior from the type of initial guess. However, the BFGS seems more stable compared to the Levenberg-Marquardt algorithm, whose behavior is always dependent on P0 in all the considered cases. The values of this parameter assumed by all techniques are, in any case, indicative of good data fitting. As far as P0 is concerned, it becomes clear that this solution for the Jonscher parameterization results inadequate as the noise level increases.

Concerning the last case of concrete we considered, characterized with an MC equal to 12%, it was studied numerically by analyzing exclusively the case of the highest noise level, $\sigma = 0.1$, with the aim to evaluate the numerical performance of the various methods we considered in determining Jonscher's parameterization, in the extreme case for high noise in the data. From results reported in Figure (10) and Tables (17), (18), we can observe that the overall behavior of the various methods carried out in the previous cases is confirmed, with the analytical P0 method providing the worst performance (MAPE(Re) = 13.5%, MAPE(Im)=29.9%). Among the nonlinear optimization methods, the Levenberg-Marquardt method once again exhibited slightly worse error metrics than those provided by the BFGS and Nelder-Mead methods (which provided the same results). However, the parametrization computed with all methods reproduced the trend of the data also in this case. Crucially, all optimization methods successfully reproduced data trends, with consistent superiority in imaginary-part fitting (Nelder-Mead/BFGS MAE(Im) = 0.179 vs MAE(Re) = 0.339). The 15× reduction in MAPE(Im) compared to P0 underscores and confirms the indispensability of numerical optimization for noisy, high-moisture scenarios. Finally, regarding the CPU Time, the data reported in Table (18) confirms for this parameter the behavior that we have deduced from all the previously considered cases. In fact, Nelder-Mead maintains its efficiency advantage, being ≈4.6× faster than Levenberg-Marquardt and 3.7× faster than BFGS. The efficiency hierarchy we noted in the above cases persists also in this case. Figure (11) show the behavior of the MAPE related to the fitting solution computed by the Nelder-Mead, BFGS quasi-Newton, and Levenberg-Marquardt algorithms as a function of the frequency f_2 used to evaluate the initial guess solution P0, and of P0 itself, for the MC=12% and noise level $\sigma = 0.1$. The considerations we made for the other cases examined can be exactly extended for this last case as well.

Finally, it is worth emphasizing that the observed variations in the fitting performance of all the nonlinear optimization algorithms considered in our analysis under different initial guesses and noise levels suggest that the objective function $\Phi(\theta)$ exhibits a nontrivial topology with multiple stationary points [41].

B. REAL DATA

All the considerations regarding the behavior of the fitting performance of the Nelder-Mead, BFGS quasi-Newton, and Levenberg-Marquardt techniques, as well as those about the analytical methodology for determining the Jonscher parameterization described in the III-B4 section, resulted using artificial data, was checked by testing all of the above

TABLE 17. Jonscher parameters from Nelder-Mead, BFGS, and Levenberg-Marquardt non-linear optimization procedures and by the analytic method P0 for the noiseless and noisy synthetic Debye concrete permittivity model data, MC=12%.

$\mu_d = 0.0$ $\sigma = 0.1$	n	χ_r	$\epsilon_\infty/\epsilon_0$
PO	0.573	4.79	7.49
Nelder-Mead	0.558	7.05	5.23
Quasi-Newton	0.558	7.05	5.23
Lev-Mar	0.425	5.19	6.7

TABLE 18. MSE, MAE, MAPE, and CPU Time for the Jonscher parametrization obtained by Nelder-Mead, BFGS, and Levenberg-Marquardt nonlinear optimization procedures and by the analytic method P0 for the synthetic Debye concrete permittivity model data, MC=12%: noisy data, $\sigma = 0.1$.

	P0	Nelder Mead	BFGS	Levenberg Marquardt
MSE	0.373	0.0813	0.0813	0.121
MSE[Re]	0.279	0.0488	0.0488	0.0882
MSE[Im]	0.247	0.065	0.065	0.0831
MAE	1.67	1.63	1.63	2.42
MAE[Re]	1.12	0.339	0.339	0.5
MAE[Im]	0.976	0.179	0.179	0.347
MAPE	18	0.256	0.256	0.292
MAPE(Re)	13.5	3.67	3.67	5.16
MAPE(Im)	29.9	1.97	1.97	3.85
CPU-Time (sec.)	–	0.0124	0.0455	0.0578

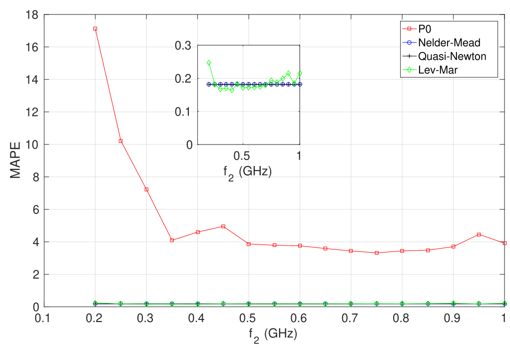

FIGURE 11. MAPE for the Jonscher parametrizations obtained by Nelder-Mead, BFGS, and Levenberg-Marquardt nonlinear optimization procedures as a function of the frequency f_2 for the Debye concrete model with MC=12%. Noise level, σ : 0.1.

TABLE 19. Jonscher parameters obtained from Nelder-Mead, BFGS, and Levenberg-Marquardt non-linear optimization procedures and by the analytic method P0 for the concrete permittivity data from [18].

	n	χ_r	$\epsilon_\infty/\epsilon_0$
P0	0.429	11.8	4.42
Nelder-Mead	0.522	8.13	6.92
BFGS	0.522	8.13	6.92
Lev-Mar	0.668	11.4	4.17

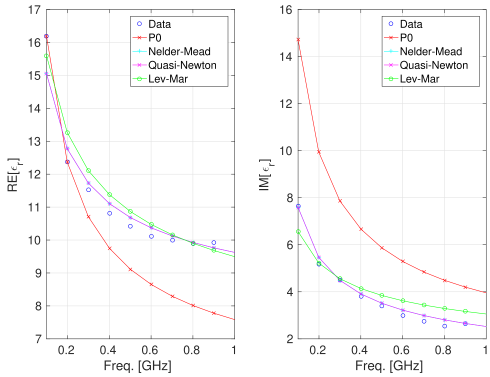

FIGURE 12. Jonscher fitting behavior obtained by Nelder-Mead, BFGS, and Levenberg-Marquardt nonlinear optimization procedures, and by the analytic method P0 for the concrete permittivity data from [18].

TABLE 20. MSE, MAE, MAPE, and CPU Time for the Jonscher parametrization obtained by Nelder-Mead, BFGS, and Levenberg-Marquardt nonlinear optimization procedures and by the analytic method P0 for the concrete permittivity data from [18].

	P0	Nelder Mead	BFGS	Levenberg Marquardt
MSE	1.17	0.147	0.147	0.238
MSE[Re]	0.47	0.135	0.135	0.154
MSE[Im]	1.07	0.0576	0.0576	0.181
MAE	3.45	1.47	1.47	2.38
MAE[Re]	1.27	0.381	0.381	0.726
MAE[Im]	2.96	0.314	0.314	0.424
MAPE	28.5	0.151	0.151	0.486
MAPE(Re)	12.5	3.03	3.03	6.13
MAPE(Im)	73.9	2.57	2.57	3.71
CPU-Time (sec.)	–	0.0822	0.875	0.263

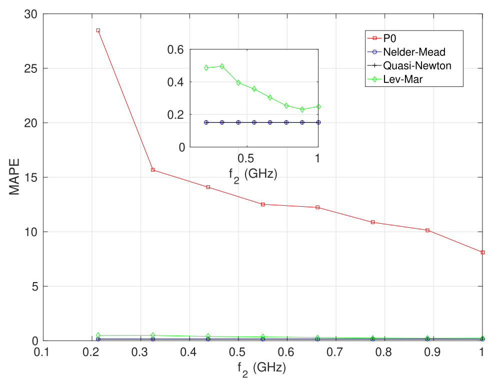

FIGURE 13. MAPE for the Jonscher parametrizations obtained by Nelder-Mead, BFGS, and Levenberg-Marquardt nonlinear optimization procedures as a function of the frequency f_2 for the concrete permittivity data from [18].

procedures on real data. To this purpose, we consider the complex permittivity experimental measurement [18] carried out on a block of concrete with a water-to-cement ratio of 0.55 (a typical concrete suitable for many general construction applications characterized by moderate strength [18]), age of three days and maximum heterogeneity size equal to 30 mm.

The number of samples exploited in our computation was $m = 10$, while $f_1 = 0.1$ GHz and $f_2 = 0.1988$ GHz were the frequencies employed to compute the analytic solution P0. Results reported in Tables (19), (20), and Figure (12) regarding the coefficients of the parameterization, the metrics related to the goodness of fit and its behavior concerning the actual data confirm the conclusions we derived in connection with the analysis carried out in section IV-A; the analytical P0 method exhibited severe limitations with unacceptable error metrics: a MAPE of 28.5% (comprising 12.5% for real and 73.9% for imaginary components) and a MAE of 3.45. In stark contrast, Nelder-Mead and BFGS demonstrated remarkable efficacy, achieving a MAPE of 0.151% (3.03% real, 2.57% imaginary) and MAE of 1.47.

While Levenberg-Marquardt remained viable with 0.486% MAPE, its performance was measurably inferior to both Nelder-Mead and BFGS across all metrics, particularly in imaginary component accuracy where its MSE[Im] of 0.181 was 3.14× higher than the 0.0576 achieved by the leading methods. About the CPU Time, we can observe that Nelder-Mead resulted in 10.6× faster than BFGS and 3.2× quicker than Levenberg-Marquardt. This significant temporal differential, consistent with the observations made in section IV-A, establishes Nelder-Mead as the optimal balance between precision and efficiency.

V. CONCLUSION

Despite the widespread use of Jonscher universal dielectric response to model the EM characteristic of concrete, at the best of our knowledge, no work in the literature has focused on the problem of choosing the most appropriate numerical method to fit it to the measured permittivity data and on the related issue of the robustness of initial guess solution by which feds the nonlinear optimization procedure selected to solve this fitting problem.

In this work, the performances of Nelder-Mead, Broyden-Fletcher-Goldfarb-Shanno quasi-Newton, and Levenberg-Marquardt optimization algorithms [41], considered due to their popularity and broad adoption within numerical software packages, have been compared to answer the above questions. In addition to the above optimization techniques, an analytical solving procedure, proposed in [28] and named P0, was considered in our study, which has also been used as an initial guess for all the nonlinear procedures mentioned above. The conducted analysis of synthetic and real data reveals that the Nelder-Mead and BFGS methods are the most robust in terms of the initial guess choice and noise in the data, providing a substantially stable solution concerning these variables compared to the Levenberg-Marquardt method, which exhibits sensitivity both to initial guess and noise. Regarding the results provided by the analytic solution method P0, they are comparable to that of other considered nonlinear optimization algorithms only in the case of noise-free data. However, our numerical analysis indicates that it can be effectively utilized as an initial guess solution for all the aforementioned nonlinear procedures.

In terms of CPU time, although the BFGS is slower than the Nelder-Mead method, from a practical perspective, the absolute value of the latter, a few fractions of a second, actually makes this parameter of secondary importance in choosing which method to employ to evaluate the optimal parameterization for the Jonscher model. Based on our numerical experiment campaign, since the error metrics of the two methods in question are the same, application situations may arise in which algorithmic simplicity could be the prevailing criterion. In this sense, the Nelder-Mead method should be preferred over the BFGS method by practitioners or researchers in the field due to its inherent computational characteristics [41] that make it suitable for hardware implementation on low-resource embedded or real-time systems [59].

As a general consideration valid for all the above methods descending from the numerical experiments we conducted, there appears to be a direct link between the quality of the fitting provided by the Jonscher parameterization and the MC of the concrete considered, which becomes less effective as the MC parameter increases. Additionally, by our analysis, a further qualitative relationship can be inferred between the water-to-cement ratio, concrete age, and the Jonscher parameters. Higher moisture content, which typically corresponds to a higher water-to-cement ratio or younger concrete age, tends to increase the imaginary component of the complex permittivity and leads to elevated values of χ_r and $\epsilon_\infty/\epsilon_0$ in the Jonscher model. To conclude, we point out that the results of this study were specifically directed toward characterizing concretes and that their direct applicability to other heterogeneous dielectrics, such as soils or polymers, may be limited since these materials have microscopic structures that may necessitate the use of alternative constitutive models, also for predicting their shielding performance [60]. Future work will be devoted both to exploring the influence of factors such as temperature, aggregate type, and curing conditions on the complex permittivity $\epsilon_r(\omega)$ and to develop an automatic procedure for selecting the pair of frequencies (f_1, f_2) used in the analytical computation of the initial guess P0. In particular, we will consider strategies based on minimizing the MAPE of P0 over the observed permittivity data.

REFERENCES

[1] B. Kanagaraj, N. Anand, R. Samuvel Raj, and E. Lubloy, "Techno-socio-economic aspects of Portland cement, geopolymer, and limestone calcined clay cement (LC3) composite systems: A-state-of-art-review," *Construct. Building Mater.*, vol. 398, Sep. 2023, Art. no. 132484.

[2] K. Kaptan, S. Cunha, and J. Aguiar, "A review: Construction and demolition waste as a novel source for CO_2 reduction in Portland cement production for concrete," *Sustainability*, vol. 16, no. 2, p. 585, Jan. 2024.

[3] D. N. Korotkikh, V. A. Dorf, D. E. Kapustin, and L. Z. Zeid Kilani, "Quality control of monolithic concrete placement in a structure with a non-removable steel-fiber concrete formwork," *Construct. Mater.*, vol. 11, pp. 31–39, Dec. 2024.

[4] G. Angiulli, P. Burrascano, M. Ricci, and M. Versaci, "Advances in the integration of artificial intelligence and ultrasonic techniques for monitoring concrete structures: A comprehensive review," *J. Compos. Sci.*, vol. 8, no. 12, p. 531, Dec. 2024.

[5] G. Angiulli, S. Calcagno, F. La Foresta, and M. Versaci, "Concrete compressive strength prediction using combined non-destructive methods: A calibration procedure using preexisting conversion models based on Gaussian process regression," *J. Compos. Sci.*, vol. 8, no. 8, p. 300, Aug. 2024.

[6] K. Bouzaffour, B. Lescop, P. Talbot, F. Gallée, and S. Rioual, "Development of an embedded UHF-RFID corrosion sensor for monitoring corrosion of steel in concrete," *IEEE Sensors J.*, vol. 21, no. 10, pp. 12306–12312, May 2021.

[7] D. Mair, M. Fischer, J. Konzilia, M. Renzler, and T. Ussmueller, "Evolutionary optimization of antennas for structural health monitoring," *IEEE Access*, vol. 11, pp. 4905–4913, 2023.

[8] J. R. Tenório Filho, J. Goethals, R. Aminzadeh, Y. Abbas, D. E. V. Madrid, V. Cnudde, G. Vermeeren, D. Plets, and S. Matthys, "An automated wireless system for monitoring concrete structures based on embedded electrical resistivity sensors: Data transmission and effects on concrete properties," *Sensors*, vol. 23, no. 21, p. 8775, Oct. 2023.

[9] D. Telfah, H. Al-Mattarneh, R. Ismail, A. Rawashdeh, M. Aljamal, and M. Dahim, "Development of permittivity sensor for advanced in situ testing and evaluation of building material," in *Proc. 21st Int. Multi-Conf. Syst., Signals Devices (SSD)*, Apr. 2024, pp. 164–169.

[10] U. B. Halabes, A. Sotoodehnia, K. R. Maser, and E. Kausel, "Modeling of the electromagnetic properties of concrete," *Mater. J.*, vol. 90, no. 6, pp. 552–563, 1993.

[11] R. H. Haddad and I. L. Al-Qadi, "Characterization of Portland cement concrete using electromagnetic waves over the microwave frequencies," *Cement Concrete Res.*, vol. 28, no. 10, pp. 1379–1391, Oct. 1998.

[12] S. N. Kharkovsky, M. F. Akay, U. C. Hasar, and C. D. Atis, "Measurement and monitoring of microwave reflection and transmission properties of cement-based specimens," *IEEE Trans. Instrum. Meas.*, vol. 51, no. 6, pp. 1210–1218, Dec. 2002.

[13] U. C. Hasar, "Nondestructive and noncontacting testing of hardened mortar specimens using a free-space method," *J. Mater. Civil Eng.*, vol. 21, no. 9, pp. 484–493, Sep. 2009.

[14] F. Tosti and E. Slob, "Determination, by using GPR, of the volumetric water content in structures, substructures, foundations and soil," in *Civil Engineering Applications of Ground Penetrating Radar*. Cham, Switzerland: Springer, 2015, pp. 163–194.

[15] G. Klysz and J.-P. Balayssac, "Determination of volumetric water content of concrete using ground-penetrating radar," *Cement Concrete Res.*, vol. 37, no. 8, pp. 1164–1171, Aug. 2007.

[16] K. L. Chung and S. Kharkovsky, "Monitoring of microwave properties of early-age concrete and mortar specimens," *IEEE Trans. Instrum. Meas.*, vol. 64, no. 5, pp. 1196–1203, May 2015.

[17] A. Kalogeropoulos, J. van der Kruk, J. Hugenschmidt, J. Bikowski, and E. Brühwiler, "Full-waveform GPR inversion to assess chloride gradients in concrete," *NDT E Int.*, vol. 57, pp. 74–84, Jul. 2013.

[18] A. Robert, "Dielectric permittivity of concrete between 50 MHz and 1 GHz and GPR measurements for building materials evaluation," *J. Appl. Geophys.*, vol. 40, nos. 1–3, pp. 89–94, 1998.

[19] M. Jamil, M. K. Hassan, H. M. A. Al-Mattarneh, and M. F. M. Zain, "Concrete dielectric properties investigation using microwave nondestructive techniques," *Mater. Struct.*, vol. 46, nos. 1–2, pp. 77–87, Jan. 2013.

[20] S. Gao, K. L. Chung, A. Cui, M. Ghannam, J. Luo, L. Wang, M. Ma, and Z. Liao, "Accurate strength prediction models of ordinary concrete using early-age complex permittivity," *Mater. Struct.*, vol. 54, no. 4, p. 172, Aug. 2021.

[21] H. Ju, L. Xing, A. H. Ali, I. E. El-Arab, A. E. A. Elshekh, M. Abbas, N. Abdullah, S. Elattar, A. Hashmi, E. Ali, and H. Assilzadeh, "Predicting concrete strength early age using a combination of machine learning and electromechanical impedance with nano-enhanced sensors," *Environ. Res.*, vol. 258, Oct. 2024, Art. no. 119248.

[22] W. Tuvayanond, V. Kamchoom, and L. Prasittisopin, "Efficient machine learning for strength prediction of ready-mix concrete production (prolonged mixing)," *Construct. Innov.*, Jul. 2024.

[23] L. Prasittisopin and W. Tuvayanond, "Machine learning for strength prediction of ready-mix concretes containing chemical and mineral admixtures and cured at different temperatures," in *Proc. 6th Int. Conf. Civil Eng. Archit.*, Singapore, 2024, pp. 242–249.

[24] Y. Zhong, P. Wang, B. Zhang, Y. Wang, T. Liu, X. Li, and Y. Niu, "Research on detection method of concrete compressive strength based on dielectric properties," *J. Building Eng.*, vol. 76, Oct. 2023, Art. no. 107090.

[25] S. Farhana, N. Qaddoumi, and S. Yehia, "Multiphase dielectric mixing model for concrete mixtures," *IEEE Access*, vol. 11, pp. 142884–142892, 2023.

[26] B. Zhang, Y. Ni, and Y. Zhong, "Theoretical derivation of and experimental investigations into the dielectric properties modeling of concrete," *J. Mater. Civil Eng.*, vol. 35, no. 3, Mar. 2023, Art. no. 04022445.

[27] J. Calderwood, "Dielectric relaxation in solids," *J. Electrostatics*, vol. 18, no. 3, pp. 346–348, Oct. 1986.

[28] T. Bourdi, J. E. Rhazi, F. Boone, and G. Ballivy, "Application of Jonscher model for the characterization of the dielectric permittivity of concrete," *J. Phys. D, Appl. Phys.*, vol. 41, no. 20, Oct. 2008, Art. no. 205410.

[29] T. Bourdi, F. Boone, J. E. Rhazi, and G. Ballivy, "Use of Jonscher model for estimating the thickness of a concrete slab by technical GPR," *Prog. Electromagn. Res. M*, vol. 28, pp. 89–99, 2013.

[30] K. Chung, L. Yuan, S. Ji, L. Sun, C. Qu, and C. Zhang, "Dielectric characterization of Chinese standard concrete for compressive strength evaluation," *Appl. Sci.*, vol. 7, no. 2, p. 177, Feb. 2017.

[31] A. Ihamouten, K. Chahine, V. Baltazart, G. Villain, and X. Derobert, "On variants of the frequency power law for the electromagnetic characterization of hydraulic concrete," *IEEE Trans. Instrum. Meas.*, vol. 60, no. 11, pp. 3658–3668, Nov. 2011.

[32] K. Y. Lee, Y.-N. Phua, S.-K. Lim, K. Y. You, and E. M. Cheng, "Determination of density and compressive strength of lightweight foamed concrete using frequency domain approach," *Microw. Opt. Technol. Lett.*, vol. 63, no. 8, pp. 2153–2159, Aug. 2021.

[33] S. Huang, K. L. Chung, K. Zheng, and X. Liu, "An improved Jonscher model for broadband dielectric characterization of cement composites," in *Proc. IEEE Int. Symp. Antennas Propag. (ISAP)*, Oct. 2023, pp. 1–2.

[34] A. K. Jonscher, "The 'universal' dielectric response. I," *IEEE Elect. Insul. Mag.*, vol. 6, no. 2, pp. 16–22, 1990.

[35] A. K. Jonscher, "The 'universal' dielectric response. II," *IEEE Elect. Insul. Mag.*, vol. 6, no. 3, pp. 24–28, 1990.

[36] A. K. Jonscher, "The 'universal' dielectric response. III," *IEEE Elect. Insul. Mag.*, vol. 6, no. 4, pp. 19–24, Jul. 1990.

[37] A. K. Jonscher, "The universal dielectric response and its physical significance," *IEEE Trans. Electr. Insul.*, vol. 27, no. 3, pp. 407–423, Jun. 1992.

[38] *Production Volume of Cement Worldwide From 1995 to 2024 (in Billion Metric Tons)*. Accessed: Apr. 14, 2025. [Online]. Available: https://www.statista.com/statistics/1087115/global-cement-production-volume

[39] H. J. Wintle, "Linear and nonlinear data fitting for dielectrics," *IEEE Trans. Dielectr. Electr. Insul.*, vol. 9, no. 5, pp. 845–849, Oct. 2002.

[40] H. Mohammad, M. Y. Waziri, and S. A. Santos, "A brief survey of methods for solving nonlinear least-squares problems," *Numer. Algebra*, vol. 9, no. 1, pp. 1–13, 2018.

[41] L. Grippo and M. Sciandrone, *Introduction to Methods for Nonlinear Optimization*, vol. 152. Cham, Switzerland: Springer, 2023.

[42] C. Grosse, "A program for the fitting of debye, cole–cole, cole–davidson, and Havriliak–Negami dispersions to dielectric data," *J. Colloid Interface Sci.*, vol. 419, pp. 102–106, Apr. 2014.

[43] D.-L. Nguyen and T.-D. Phan, "Enhanced prediction of compressive strength in high-strength concrete using a hybrid adaptive boosting–particle swarm optimization," *Asian J. Civil Eng.*, vol. 26, no. 3, pp. 1059–1076, Mar. 2025.

[44] M. Ulucan, E. Gunduzalp, G. Yildirim, B. Alatas, and K. E. Alyamac, "Optimizing sustainable concrete compressive strength prediction: A new particle swarm optimization-based metaheuristic approach to neural network modeling for circular economy and disaster resilience," *Struct. Concrete*, vol. 26, no. 2, pp. 1226–1244, Apr. 2025.

[45] E. B. Bashier, *Practical Numerical and Scientific Computing With MATLAB and Python*. Boca Raton, FL, USA: CRC Press, 2020.

[46] S. K. Mishra and B. Ram, *Introduction to Unconstrained Optimization With R*. Cham, Switzerland: Springer, 2019.

[47] Y. Ohki, "Broadband complex permittivity and electric modulus spectra for dielectric materials research," *IEEJ Trans. Electr. Electron. Eng.*, vol. 17, no. 7, pp. 958–972, Jul. 2022.

[48] D. Barrios Puerto, "Intrinsic and extrinsic scattering and absorption coefficients new equations in four-flux and two-flux models used for determining light intensity gradients," *J. Opt. Photon. Res.*, vol. 1, no. 3, pp. 131–144, Apr. 2024.

[49] S. Abboudy, K. Alfaramawi, L. Abulnasr, and B. K. Hefny, "Direct calculations of the dielectric and optical parameters of some compound semiconductors: A study using the Lorentz oscillator and Wemple-DiDomenico models," *J. Opt. Photon. Res.*, pp. 1–16, Aug. 2024.

[50] D. M. Olsson and L. S. Nelson, "The Nelder–Mead simplex procedure for function minimization," *Technometrics*, vol. 17, no. 1, pp. 45–51, Feb. 1975.

[51] J. C. Lagarias, J. A. Reeds, M. H. Wright, and P. E. Wright, "Convergence properties of the Nelder–Mead simplex method in low dimensions," *SIAM J. Optim.*, vol. 9, no. 1, pp. 112–147, Jan. 1998.

[52] P. Niegodajew, M. Marek, W. Elsner, and Ł. Kowalczyk, "Power plant optimisation—Effective use of the Nelder–Mead approach," *Processes*, vol. 8, no. 3, p. 357, Mar. 2020.

[53] D. C. Liu and J. Nocedal, "On the limited memory BFGS method for large scale optimization," *Math. Program.*, vol. 45, nos. 1–3, pp. 503–528, Aug. 1989.

[54] L. Nazareth, "A relationship between the BFGS and conjugate gradient algorithms and its implications for new algorithms," *SIAM J. Numer. Anal.*, vol. 16, no. 5, pp. 794–800, Oct. 1979.

[55] M. R. Osborne, "Nonlinear least squares—The Levenberg algorithm revisited," *J. Austral. Math. Soc. Ser. B. Appl. Math.*, vol. 19, no. 3, pp. 343–357, Jun. 1976.

[56] M. I. Lourakis, "A brief description of the Levenberg–Marquardt algorithm implemented by levmar," *Found. Res. Technol.*, vol. 4, no. 1, pp. 1–6, 2005.

[57] Z. Khan, S. Chawla, and D. Dave, "A note on comparison of nonlinear least squares algorithms," *ACM SIGNUM Newslett.*, vol. 25, no. 2, pp. 10–18, Jul. 1990.

[58] V. Beiranvand, W. Hare, and Y. Lucet, "Best practices for comparing optimization algorithms," *Optim. Eng.*, vol. 18, no. 4, pp. 815–848, Dec. 2017.

[59] U. Zabit, F. Bony, and T. Bosch, "Optimisation of the Nelder–Mead simplex method for its implementation in a self-mixing laser displacement sensor," in *Smart Sensors and Sensing Technology*. Berlin, Germany: Springer, 2008, pp. 381–399.

[60] M. Priya, A. A. Suresh, M. Dhavamurthy, and A. V. Deepa, "Theoretical studies on γ-photon/neutron shielding characteristics of RE3+Co-doped borate, phosphate, and silicate glass systems," *J. Opt. Photon. Res.*, pp. 1–13, May 2024.

GIOVANNI ANGIULLI (Senior Member, IEEE) received the Ph.D. degree in electronic engineering and computer science from the University of Naples Federico II, in 1998. In 1999, he joined the Mediterranea University of Reggio Calabria, as an Adjunct Professor of electrical engineering. His research interests include numerical methods and functional analysis techniques in electromagnetics and electrical engineering. He is an IEICE Member. In recognition of his contributions, he has been awarded by the IEEE Access Editorial Board and staff as an Outstanding Associate Editor of 2018 for IEEE ACCESS.

MARIO VERSACI (Senior Member, IEEE) received the Laurea degree in civil engineering from the Mediterranea University of Reggio Calabria, Italy, in 1994, the Ph.D. degree in electronic engineering, in 1999, and the Laurea degree in mathematics from the University of Messina, Italy, in 2013. He is currently an Associate Professor of electrical engineering and the Scientific Head of the NDT/NDE Laboratory, Mediterranea University of Reggio Calabria. His research interests include soft computing techniques for non-destructive testing (NDT)/non-destructive evaluation (NDE) and image processing. He is a member of Italian Society for Industrial and Applied Mathematics.